Lebanon Solar Rooftop Potential Assessment Using Buildings Segmentation From Aerial Images

Hasan Nasrallah , Abed Ellatif Samhat , Yilei Shi, *Member, IEEE*, Xiao Xiang Zhu , *Fellow, IEEE*, Ghaleb Faour , and Ali J. Ghandour

Abstract—Estimating solar rooftop potential at a national level is a fundamental building block for every country to utilize solar power efficiently. Solar rooftop potential assessment relies on several features such as building geometry, location, and surrounding facilities. Hence, national-level approximations that do not take these factors into deep consideration are often inaccurate. This article introduces Lebanon's first comprehensive footprint and solar rooftop potential maps using deep learning-based instance segmentation to extract buildings' footprints from satellite images. A photovoltaic panels placement algorithm that considers the morphology of each roof is proposed. We show that the average rooftop's solar potential can fulfill the yearly electric needs of a single-family residence while using only 5% of the roof surface. The usage of 50% of a residential apartment rooftop area would achieve energy security for up to 8 households. We also compute the average and total solar rooftop potential per district to localize regions corresponding to the highest and lowest solar rooftop potential yield. Factors such as size, ground coverage ratio and PV_{out} are carefully investigated for each district. Baalbeck district yielded the highest total solar rooftop potential despite its low built-up area. While Beirut capital city has the highest average solar rooftop potential due to its extremely populated urban nature. Reported results and analysis reveal solar rooftop potential urban patterns and provides policymakers and key stakeholders with tangible insights. Lebanon's total solar rooftop potential is about 28.1 $TWh/year$, two times larger than the national energy consumption in 2019.

Index Terms—Deep learning, earth observing system, image segmentation, solar energy.

I. INTRODUCTION

BUILDING footprints extraction from aerial imagery is essential for many urban applications, including geographical databases, land use, and change analysis. Fully automated extraction and recognition of buildings' footprints geometries can help estimate the solar potential of every rooftop. Estimating rooftops' solar potential provides more insight into how a given

Hasan Nasrallah and Abed Ellatif Samhat are with the Faculty of Engineering - CRSI, Lebanese University, Hadat, Lebanon (e-mail: hnasrallah@geogroup.ai; samhat@ul.edu.lb).

Yilei Shi and Xiao Xiang Zhu are with the Technical University of Munich, 80333 Munich, Germany (e-mail: yilei.shi@tum.de; xiaoxiang.zhu@dlr.de).

Ghaleb Faour and Ali J. Ghandour are with the National Center for Remote Sensing - CNRS, Riad El-Solh 1107 2260, Beirut, Lebanon (e-mail: gfaour@cnrs.edu.lb; aghandour@cnrs.edu.lb).

country can efficiently utilize renewable resources for solar power generation.

Solar power harvesting paves the way for ensuring a greener future and a better economic status. The first step to accomplish this task is acquiring rooftop geometries that we tackle via satellite imagery analysis and object segmentation.

Segmentation of urban aerial imagery is currently undergoing significant attention in the research community and notable development efforts in the industry. Remote sensing images are usually complex and characterized by significant intraclass variations, and often low interclass variations [1].

Deep learning significantly reduces the time and cost required for aerial imagery segmentation due to its capabilities in automatically extracting features and patterns present in large scenes. This work uses deep convolutional neural networks to extract rooftop geometries and obtain Lebanon's first complete and comprehensive urban map.

We then use a solar panel placement algorithm that considers the area and morphology of every rooftop to estimate the number of panels that can fit on top. Automated solar rooftop potential estimation is made feasible given the corresponding photovoltaic (PV) power generated per unit of the installed panels.

The contribution of this article is threefolds:

1) *design the first complete Lebanese buildings' footprints map using instance segmentation from satellite images;*
2) *present also the first Lebanese solar rooftop potential map by estimating the solar potential of every rooftop morphology;*
3) *thorough analysis and insights of solar rooftop potential trends for each Lebanese district.*

The rest of the article is organized as follows: Section II shows the literature review related to the use of deep learning models for building footprints detection and solar estimation from aerial images. We present in Section III the TUM dataset created for the scope of segmenting Lebanese buildings. Buildings footprints map is discussed in Section IV. Solar rooftop potential assessment approach is presented in Section V and associated results are revealed in Section VI. Finally, Section VII concludes the article.

II. RELATED WORK

A. Buildings' Segmentation

Several techniques tackle the problem of buildings segmentation from aerial imagery. In [20], the authors use gated graph convolutional neural networks to output a truncated signed distance map (TSDM), which is then converted into a semantic

segmentation mask of buildings. In [15], the authors propose two plug-and-play modules to generate spatial augmented, and channel augmented features for semantic segmentation from satellite images. In [14], the authors use augmentations like slicing, rescaling, and rotations, in addition to GIS data, to improve buildings' footprint extraction. However, a more direct approach is presented in Iglovikov *et al.* [11], where the authors only use a semantic segmentation network with an additional output mask designating spacing between nearby buildings to separate building instances.

Similar to Iglovikov *et al.* [11] approach, we adopted in this work a multiclass semantic UNet-like architecture, followed by a watershed postprocessing step to extract buildings' instances. However, in our proposed method, we introduced a third class, which is buildings' borders to separate nearby instances. Indeed, employing an additional buildings' borders class improved *Fscore* considerably with more than 10%. Specific details and discussions about this third class are beyond the scope of this article.

B. Solar Rooftop Potential Estimation

Solar rooftop potential estimation is currently drawing the attention of geospatial deep learning researchers due to its effectiveness in accurately predicting the potential usage of rooftops for solar power generation. Significant advances in this field have been made using statistical models, computer vision, numerical analysis, and geographic information systems. In [7], the authors use collected data about the solar radiation and the rooftop areas in Beirut city to estimate solar rooftop potential, without taking into consideration each rooftop morphology. A similar approach was conducted in [17]. In [8], authors use high precision photographic sensors mounted on a UAV to scan and create a digital surface model (DSM) for a single building. Further statistical analysis of the output DSM model, including shading, solar irradiance, and panel placement, was conducted to estimate a single roof's solar potential. Solar irradiance estimation relies on viewshed, sun-map, and skymap information. The proposed solar potential model is benchmarked with an actual solar rooftop system in production. In [5], the authors use satellite imagery to divide and segment building rooftops into sections using convolutional neural networks. They predict each section's pitch, azimuth, and shading mask and then use a greedy algorithm to place solar panels on rooftops to estimate their solar potential. A similar approach was adopted in [27] to estimate the solar potential at a city scale in China.

To the best of the authors' knowledge, there is no previous work to estimate the rooftop solar potential at a country scale for Lebanon. The presented work is thus the first attempt to produce Lebanese urban and solar rooftop potential maps. We used a deep learning model to segment rooftops from high-resolution satellite imagery (50 cm/pixel).

Unlike the work in [7] and [17], which only relies on buildings' footprint area for solar potential estimation, we devise a greedy algorithm to simulate photovoltaic (PV) panels' placement based on each rooftop morphology. Our proposed panels placement algorithm processes regularized buildings' footprints and thus return more accurate results compared to [5] and [27].
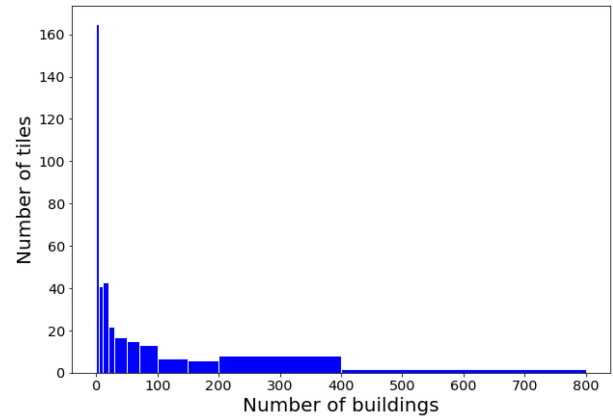

Fig. 1. Tyre Urban Map (TUM) dataset tiles' distribution per buildings count.

III. DATASET CREATION

We aim in this research to build an efficient and accurate building segmentation model from Lebanese satellite images. Since neural networks are not guaranteed to generalize well on out-of-distribution (OOD) data, a training dataset covering Lebanese populated areas with accurate buildings ground truth labels is needed. Such a dataset does not exist to our knowledge, so we created our own for this project.

The training dataset should hold a representative distribution of building types from all over Lebanon. Thus, we chose the Tyre area since it includes urban, suburban, rural, and slum areas. Tyre city itself is a dense urban city that lies within the outer ring of residential suburbs. Moreover, the chosen area has a refugee camp and vast countryside areas. Hence, the annotated training dataset does well represent the various characteristics of Lebanese areas. A segmentation model trained using this dataset would generalize well to the majority of Lebanese scenes.

We first chose a 35372 × 28874 GeoTIFF image with RGB channels taken by the GeoEye-1 satellite sensor of 50 cm/pixel resolution covering the Tyre district in the Southern Lebanon. We cropped the chosen area of interest into 1024 × 1024 chips, resulting in 338 tiles for manual annotation using the VGG-Image-Annotator tool [6]. Finally, we further cropped each tile into nonoverlapping 512 × 512 sized images while preserving each image's relative labeled polygons indices. We used nonoverlapping tiles for the training dataset to avoid any redundant data which might cause model overfitting. The final training dataset includes 1352 tiles of 512 × 512 dimensions with 10 000 buildings' objects. We refer to this dataset as Tyre Urban Map (TUM) dataset.

TUM has a balanced distribution of tiles with and without buildings [the ratio is roughly $(9:10)$]. Fig. 1 portrays the number of tiles present in the TUM dataset for each given range of buildings' count. The average count is 28 buildings per tile. Moreover, Fig. 1 shows that the tiles are distributed over areas with varying building densities ranging from rural to suburban and urban regions. Thus, the created TUM dataset is expected to generalize well for the different aspects of building land cover distributions present in Lebanon.

As for the test set, we selected 30 areas of interest (AOI) from different Lebanese regions, including Beirut, Saida, Jounieh,
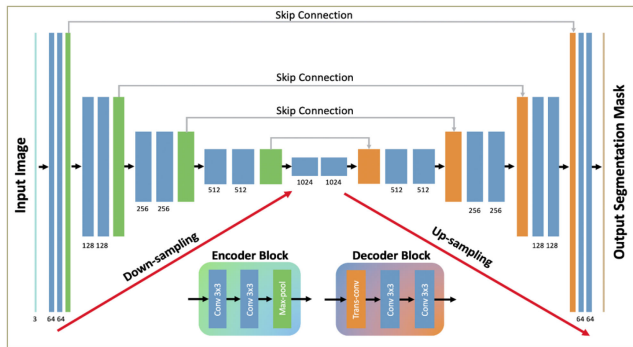
Fig. 2. Encoder-Decoder UNet Architecture used with skip connections.

Jbeil, and Tripoli. Selected AOI's encompass dense urban regions (Beirut), structured urban regions (Saida), and some rural areas. This diversity would help assess the generalizability of our model over the whole Lebanese territory. It is worth to note that we addressed, at inference time, the issue of rooftops present at tiles' edges. Test images are cropped into 1024×1024 overlapping chips with a stride value of 512. Segmentation masks are averaged, resulting in smoothly merged buildings' footprints at the edges of the tiles.

IV. BUILDINGS' FOOTPRINTS MAP

This section describes our approach to extracting buildings' rooftop polygons from satellite imagery of Lebanon. We adopt a UNet-like architecture to output semantic segmentation masks of the rooftops. To be able to separate close buildings, we also predict buildings' borders mask. The buildings' mask, buildings' spacing mask, and the buildings' borders mask are then postprocessed using the watershed algorithm [18] to separate and tag each polygon with a unique identifier and result in an instance segmentation mask.

A. Model Architecture

UNet [19] is an end-to-end, fully convolutional neural network that serves the purpose of semantic segmentation of input images over multiple classes. It consists of a contracting path [Encoder] and an expansive path [Decoder] with skip connections between symmetrical blocks of identical size. The overall architecture is a U-shaped encoder–decoder architecture as shown in Fig. 2.

The Encoder part of the architecture can be chosen from powerful and deep convolutional neural networks like Residual Nets [10], [25], Inception Nets [22], dual-path nets [4], or the newly introduced Efficient-Nets [23]. In our experiments, Efficient-Net-B3 was found to perform better, in terms of accuracy and variance, than other members of the Efficient-Net family members and other encoders like ResNet34, ResNeXt50, InceptionV4, InceptionResNetV2, and DPN92 as shown in Table I. Variance is defined as the $Fscore$ difference between the training and validation datasets. The model trained with EfficientNetB3 encoder had the best performance ($Fscore = 84.3\%$) and the best fitting on the train dataset as it achieved the lowest train/validation variance of 2.88%. Generally speaking, all trained models achieved well in terms of $Fscore$, however EfficientNets showed better fit on the dataset with lower variance than other encoders.

TABLE I
Fscore AND VARIANCE PERCENTAGES ON THE VALIDATION SET FOR
DIFFERENT BACKBONES TRAINED FOR 100 EPOCHS USING
IDENTICAL HYPERPARAMETERS

Backbone	$Fscore$ (%)	Variance (%)
ResNet34	82.8	4.33
ResNeXt50	83.7	4.24
Inception-ResNetV2	84.0	3.55
InceptionV4	84.1	4.95
DPN92	83.8	3.74
EfficientNetB2	83	2.93
EfficientNetB3	**84.3**	**2.88**
EfficientNetB4	83.8	2.97

It is evident that efficientNetB3 achieves best performance in terms of $Fscore$ and variance.

As for the loss function, we chose a normalized weighted sum of losses across all output channels. Each single channel loss is a combination of Dice loss and Binary Cross-Entropy loss [12] in order to leverage the benefits of both. It is worth to mention that we investigated a combination of Dice loss and Focal loss using EfficientNetB3 and EfficientNetB4 backbones. However, no improvement was noticed where EfficientNetB3 $Fscore$ was equal to 84.2% and EfficientNetB4 $Fscore$ equals 83.6%.

B. Training Pipeline

All models were trained for 100 epochs using Adam Optimizer [13] and the One-Cycle learning rate policy [21] starting with an initial learning rate $= \frac{0.0001}{20}$ and increases for 40 epochs in a cosine annealing manner till it reaches a maximum of 0.0001 and then decreases for the rest 60 epoch in the same annealing fashion.

During training, we used mixed precision technique and applied random augmentations. We used CutMix [26] data augmentation to further enhance our model robustness. We also used inference-time augmentations and employed postprocessing to extract instance masks from semantic segmentation. The details of those different steps are beyond the scope of this article.

Fig. 3 shows the buildings' footprints extraction model in practice applied to Jonieh City in Lebanon, with its corresponding ground truth building mask (in red) and predicted building mask (in yellow). Finally, we polygonized and regularized the output instance masks to achieve eye-pleasing regular-shape polygons as shown in Fig. 4.

V. SOLAR ROOFTOP POTENTIAL ASSESSMENT

The first step in calculating the solar potential of rooftops is to find how many solar panels can fit on each roof. However, due to the lack of critical information such as rooftops' relative slope and azimuth angle, we assume that all roofs are flat and at an orthogonal angle with the satellite sensor. Other factors like shading are also not considered due to insufficient information on the heights of all buildings in the country. In this work, we assumed a standard commercial solar panel module of dimensions (1×1.98) meters and a nominal power $P_{nominal} = 0.4$ KWp. To estimate the number of panels that can fit on each rooftop, researchers such as Eslami *et al.* [7] simply normalize
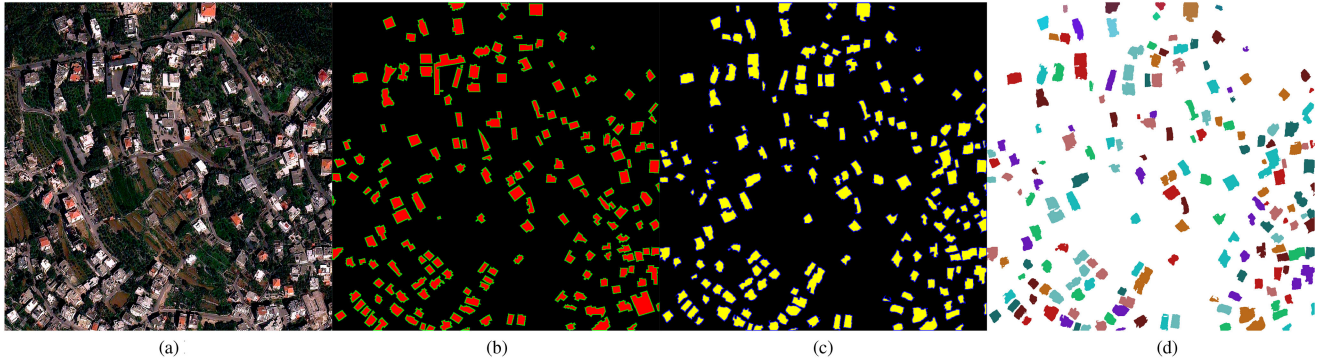
Fig. 3.   (a) Sample test image taken from Jounieh City, with (b) its corresponding ground truth buildings mask (in red) and (c) our model predicted buildings' mask (in yellow), and finally (d) postprocessing results for buildings instances segmentation. (a) Image. (b) Ground truth. (c) Prediction mask. (d) Prediction instance.

Fig. 4.   Buildings' footprint polygonization and regularization process: (a) model original output masks are first transformed into polygons and then (b) regularized to achieve buildings-like shape.

Algorithm 1: Rooftop PV Panels Fitting Algorithm.

1:    For each building footprint polygon, find its minimum bounding rectangle $BBox$.
2:    Designate longest axis of the $BBox$ as the main axis of the rooftop.
3:    Place solar panels in a greedy way inside $BBox$ along the main axis.
4:    Remove panels that extend outside the building polygon geometry.

---

the rooftop surface by the panel's area. This approach would result in an overestimation of the solar rooftop capacity since it does not take the roof's morphology into account.

For the scope of this work, we devise the PV panels fitting algorithm described in Algorithm 1 based on the work presented in [5]. The PV panels fitting algorithm is applied to the regularized buildings' footprints to avoid any segmentation irregularities present at the roof edges. Fig. 5 shows a running example of the panels fitting algorithm for a rooftop with extremely irregular shape.

Finally, we use (1) to calculate SP_r, the solar potential of every rooftop r as follows:

$$SP_r(MWh/year) = N_r * P_{nominal} * PV_{out} \qquad (1)$$

where N_r is the number of panels that fit on that roof, $P_{nominal}$ is the nominal power of the solar panel modules in (KWp), and PV_{out} is the specific photovoltaic power output of the installation in (MWh/KWp).

PV_{out} is defined as the amount of power produced per unit of the installed solar panel. In our studies, we used PV_{out} data obtained from the World Bank Global Solar Atlas 2.0 [9]. The acquired data comprise a mapping of yearly averaged PV_{out} values for every $1 Km^2$ grid tile across the whole Lebanese territory. The PV_{out} heatmap for Lebanon is shown in Fig. 6. For every rooftop, we locate the corresponding tile within the PV_{out} map and fetch its relative PV_{out} value in (MWh/KWp). Thus, we base our calculation on a more accurate and precise PV_{out} map than other studies that use fixed PV_{out} values [7].

VI. RESULTS

In this section, we present analysis and results for the solar rooftop potentials on two levels: 1) rooftop level and 2) district level. At the rooftop level, we reveal that the average roof's solar potential is sufficient enough to cover most of the energy needs of Lebanese households and achieve a sense of energy security. At the district level, we compute the total and average solar rooftop potentials per district and compare these values with the maximum hypothetical capacity of each district.

A. Household Energy Security

For every rooftop, we fetch its relative PV_{out} value and fit the maximum number of panels. Since we use a greedy algorithm for the solar panels' placement, we then calculate the maximum theoretical solar rooftop potential capacity. Fig. 7 shows the PV panels fitting algorithm and solar potential calculation scheme in action for a demo house where 45 panels were placed which corresponds to 30.4398 $MWh/year$.

In practical situations, fewer solar panels could be placed due to various parameters, including objects usually available on the roof (such as roof tanks and solar water heaters, among others), inclined roof slope, and the requirement of leaving sufficient room for service and emergency access. We multiply the number of fitted solar panels with a utilization factor U to account for this effect. Although studies in the literature [3], [7] report results for only 50% and 75% utilization factors, for the scope of this work, we experimented with several utilization factors in the following results sections, where $U \in [0.1, 0.25, 0.5, 0.75, 1]$.

The histogram presented in Fig. 8 shows buildings' distribution across solar rooftop potential bins in $MWh/year$. Those results are computed assuming a 50% utilization factor U.

Rooftops' solar potential that falls in the range $[1, 10]$ MWh/year account for around 21% of the distribution. Those are
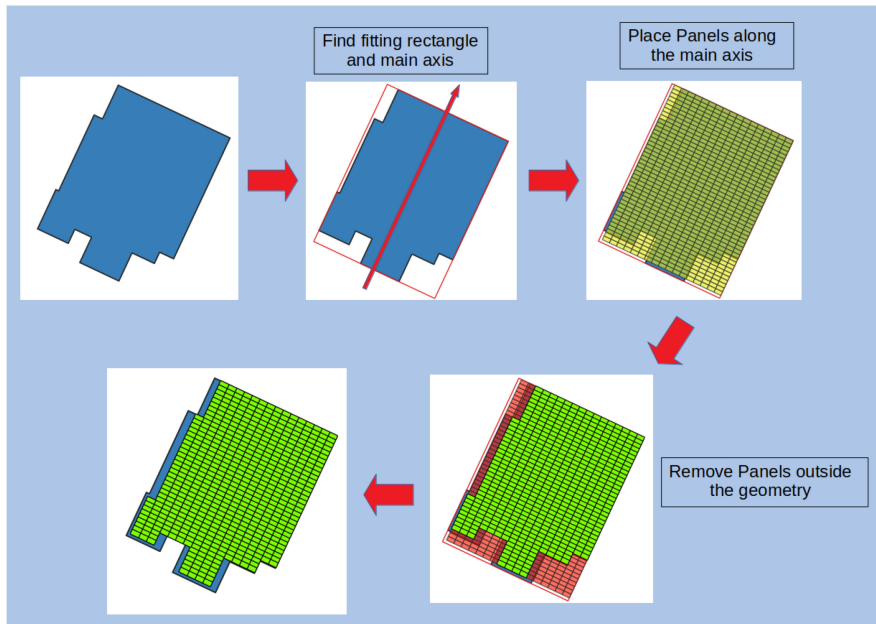
Fig. 5. Solar panels fitting algorithm. The algorithm takes into consideration the morphology and the geometry of the roof. Solar panels are greedily placed along the longest axis of the building footprint to maximize the number of panels fitted inside the it's geometry. Panels extending outside the geometry are removed, and the remaining panels are taken into consideration for the solar potential calculation.
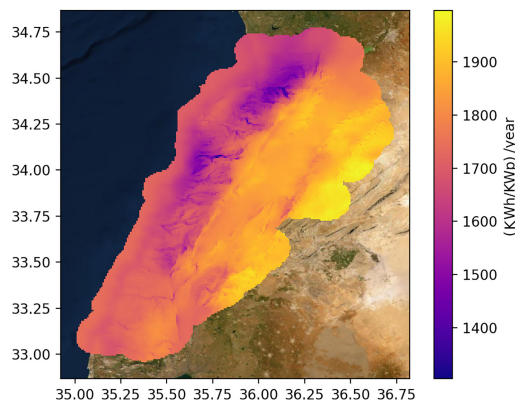

Fig. 6. Lebanese PV_{out} heatmap used for solar rooftop calculation. PV_{out} is an average of the yearly production normalized to 1 KWp of installed capacity. It is clear that areas within the East Beqaa Valley involve high potentials for solar energy generation.

Fig. 7. Panel fitting and solar potential calculation for a demo rooftop. The algorithm deduces that the roof maximum theoretical capacity holding is 45 panels which corresponds to 30.4398 MWh/year. Small portion of the roof contours were left empty due to the inability of fitting a whole panel module in the remaining small area.
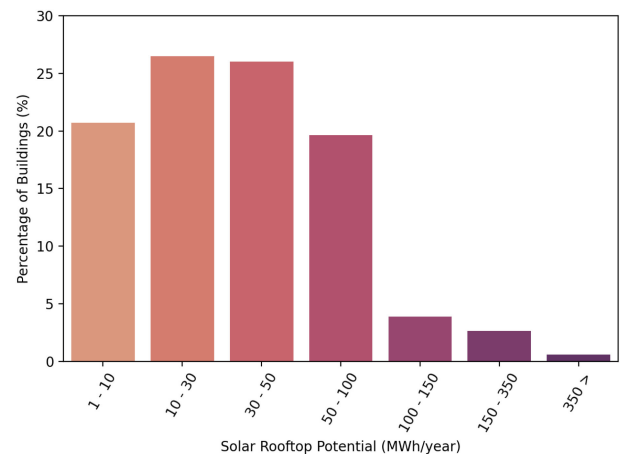

Fig. 8. Buildings' distribution across different bins of solar rooftop potential using $U = 50\%$. More than half of the rooftops can produce energy in the range $[10, 50]$ MWh/year. While remaining 40% of the rooftops are equally distributed among the two intervals: $[1, 10]$ and $[50, 100]$ MWh/year.

usually homes characterized with rooftops of a smaller surface or lower PV_{out} value than the rest of the distribution. On the other edge, 7% of the buildings are associated with high expected solar rooftop potential, between 100 MWh/year and 350 MWh/year. Values above 350 MWh/year are primarily due to segmentation errors in high density areas such as slums where multiple nearby building footprints are merged.

More than half of the distribution (53% of the buildings) can leverage a total solar rooftop potential in the range $[10, 50]$ MWh/year. Finally, 19% of the buildings have rooftops capable of producing a high total solar potential between $[50, 100]$ MWh/year.

For the scope of this work, average solar rooftop potential (ASP) is defined as the mean of the solar rooftop potential of all

Utilization Factor	Average rooftop Solar Potential	Standard Error
10%	9.747	±6.22
25%	22.21	±14.87
50%	40.81	±27.67
75%	58.11	±38.54
100%	74.29	±48.09

ASP is defined as the mean of the solar rooftop potential of all buildings across Lebanon.

buildings across Lebanon. Table II presents ASP in MWh/year for various utilization factors with the associated standard error (SE) value. SE is defined in (2). Large observed SE values are attributed to the wide variety of solar rooftop potential in the buildings' distribution set as shown earlier in Fig. 8

$$SE = \frac{\sigma}{\sqrt{n}} \tag{2}$$

where σ is the sample standard deviation and n is the number of samples.

A recent survey [2] shows that households in Lebanon consume on average 5.41 MWh/year. A low 10% utilization factor can accommodate an average of 9.747 MWh/year, which corresponds to 180% of the average household's electricity consumption per year. Using only around 5% of the roof surface would allow single-family residences to significantly cut their electricity bills and meet near-net zero energy building (near-$NZEB$) targets [24]. And also, sell surplus energy back to the grid and generate additional income, once corresponding energy regulations are updated to allow for net-metering.

Economic crisis and severe inflation witnessed since 2019 made energy security a real concern for Lebanese households. Energy security is defined as the uninterrupted availability of energy sources at an affordable price. In Lebanon, both conditions are not currently met, where most families suffer from long hours of electricity outage daily, while the average electricity bill largely exceeds the minimum wage rate. Assuming a 50% utilization factor scenario, the expected average solar rooftop potential (ASP) of a building is 40.81 (MWh/year), which is equivalent to the average yearly consumption of 7.5 households. Hence, residential apartments can achieve a significant percentage of energy security by relying on rooftop solar energy production.

B. Urban Solar Potential Factors

Lebanese territory is divided into 26 districts, where each district exhibits its own urban and topographic characteristics. As shown in Fig. 6, the specific photovoltaic power output of the installation, PV_{out} values, are not uniformly distributed across districts. A wide PV_{out} gap of more than 500 MWh/KWp is observed between locations receiving the lowest and highest amount of solar irradiation. Hence, rooftops, with the same panel
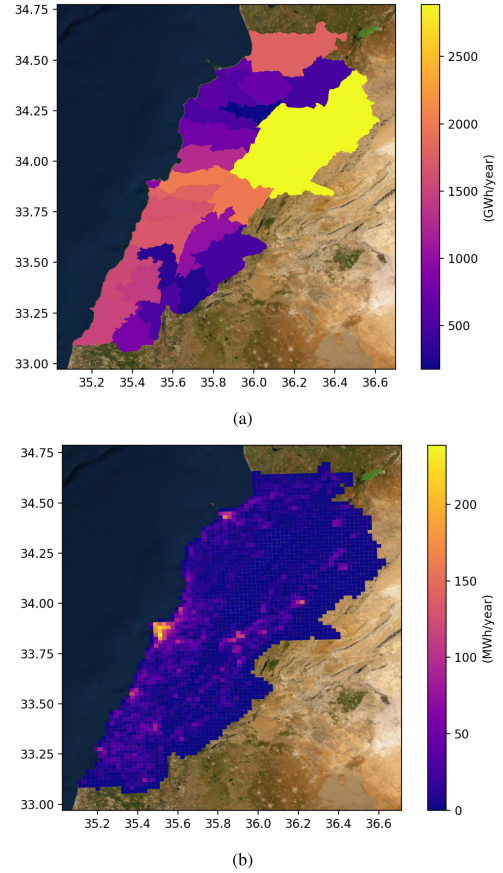

Fig. 9. (a) Total solar rooftop potential in GWh/year for different Lebanese districts using 50% Utilization factor. (b) Heatmap showing average solar rooftop potential MWh/year using a sliding window of 4 Km^2 area.

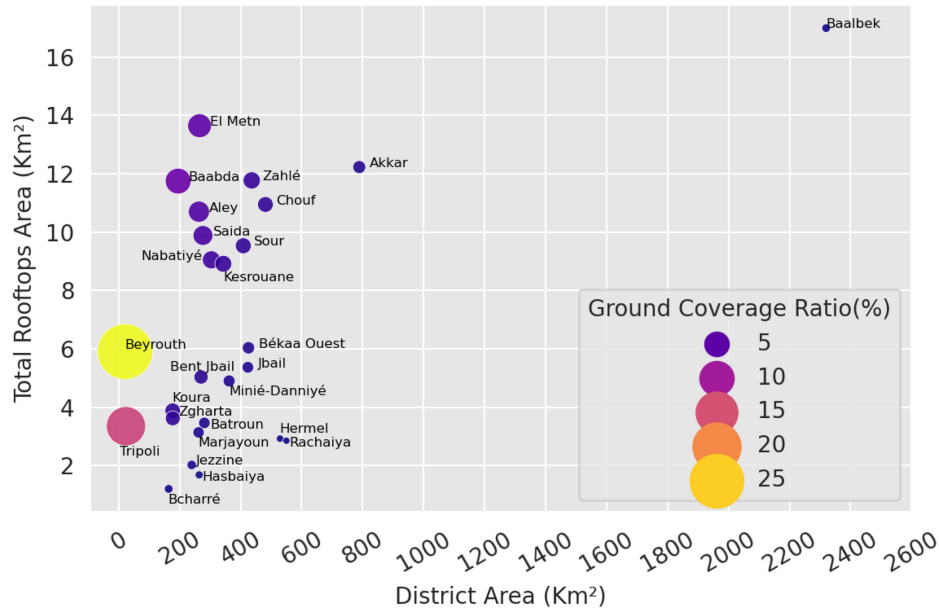Fig. 10. Lebanese districts' map [33.8547°N, 35.8623°E].

Fig. 11. Bubble Chart showing the Ground Coverage Ratio (GCR) [16] for each district. The *x*- and *y*-axes show each district surface and its corresponding rooftops area in Km^2, respectively. The bubble size designates the GCR value for each district. Beirut district shows the highest GCR value of 27%, whereas the lowest GCR value corresponds to Rachaiya district with only 0.55%.

capacity, in different districts, do not produce the same solar rooftop potential.

We calculate total solar rooftop potential in GWh/year for each district using a 50% utilization factor. We also calculate the average solar rooftop potential in MWh/year using a sliding window of size (surface) $4Km^2$. We visualize those results in Figs. 9(a) and (b), respectively. Fig. 10 is included as a reference figure to show the layout of the Lebanese districts.

Fig. 9(a) shows that Baalbeck (2885 GWh/year), El-Metn (2014 GWh/year), and Zahle (1979 GWh/year) districts have the highest total solar rooftop potentials. On the other hand, in Fig. 9(b), we observe that Baalbeck district is almost uniformly blue, which indicates that it is not well populated. Baalbeck, the largest district with the highest PV_{out} values, is indeed expected to provide the highest total solar rooftop potential. However, El-Metn district's total solar rooftop potential is only 871 GWh/year behind Baalbeck despite being 11 times smaller and witnessing lower PV_{out} values. Baalbeck belongs to the most yellowish region in Fig. 9(a) while being the most bluish one in Fig. 9(b).

To further analyze those results, we plot in Fig. 11 a bubble chart that shows the ground coverage ratio (GCR) [16] for each district. Ground coverage ratio, defined in (3), is used to assess the percentage of built-up area in each district

$$GCR = \frac{A_b}{A_T} = \frac{A_{BuildingFootprints}}{A_{District}} \quad (3)$$

where A_b is the built-up area or the total area of building footprints in a district, and A_T is the domain area and for the context of this study, it is defined as the district area.

Baalbeck district has one of the lowest GCR values of 0.73%. EL Metn district on the other hand has 5.4% GCR value, which is $7x$ larger than Baalbeck. This huge difference in built-up area justifies results observed in Fig. 9(a) and (b).

For the sake of clarity and to further expand this line of analysis, we define the maximum Hypothetical solar potential

Capacity (HC_i) of each district i, as the maximum solar potential achievable at district i, if we lay solar panels across the district whole area. HC_i is a hypothetical value, where we assume that the district topology is flat. HC_i is used in the scope of this work as an indicator to assess the amount of solar potential that can be produced at each district level. HC_i values are reported in Table III.

Baalbeck, Lebanon's largest district, has a maximum hypothetical capacity of 845 TWh/year. However, due to the low built-up area in the region, solar potential cannot be efficiently exploited at the rooftop level. An alternative solution we suggest here is to install large solar farms in Baalabek district to avail solar potentials.

C. District-Level Analysis

Beirut solar map [7] reports 195 MWp as the nominal capacity of the city for a 50% Utilization factor and 295 MWp for a 75% Utilization Factor. Our findings shows that the nominal capacity of the city is 285 and 427 MWp for 50% and 75% Utilization factors, respectively. The difference is due to the following factors: 1) assumption in [7] that every 8 sqm yields a total of 1 KWp. While in our work, we used a standard commercial PV panel with an area equal to 1.98 sqm and nominal power equal to 0.4 KWp, which is $1.6\times$ larger. Thus, results in Eslami *et al.* [7] should be weighted by a $1.6\times$ factor for a fair comparison. 2) The difference between the newly weighted values (312 and 472 MWp) and our findings (285 and 427 MWp) is less than 10%. 3) PV panel placement is not employed in [7] and thus roof morphology is not taken into consideration which ended up with an overestimation of the actual solar rooftop potential of the city.

The capital city (Beirut) and the economic capital (Tripoli) have fairly mid-range total rooftop solar potential with 907 and 516 GWh/year, respectively. These two districts have the most glowing spots on the heatmap shown in Fig. 9(b) and exhibit the

TABLE III
AVERAGE SOLAR ROOFTOP POTENTIAL VALUES (ASP IN $MWh/year$) AND TOTAL SOLAR ROOFTOP POTENTIAL VALUES (TSP IN GWH/YEAR) PER DISTRICT WHILE VARYING UTILIZATION FACTOR BETWEEN 10% AND 100%

District	Average Solar rooftop Potential (ASP in $MWh/year$)					Total Solar rooftop Potential (TSP in $GWh/year$)					Hypothetical Capacity (HC in $TWh/year$)	$\%\frac{TSP}{HC}$
	Utilization Factor											
	10%	25%	50%	75%	100%	10%	25%	50%	75%	100%		
Baalbek	7	17	35	53	70	577	1442	2885	4328	**5771**	**845**	0.68
El Metn	9	22	45	68	91	402	1007	2014	3022	4029	74	5.44
Zahlé	9	24	49	74	98	395	989	1979	2968	3958	139	2.85
Baabda	10	27	54	81	109	357	893	1786	2679	3572	50	7.14
Akkar	6	15	31	46	62	355	887	1775	2662	3550	235	1.51
Chouf	7	18	37	56	75	335	839	1679	2519	3359	141	2.38
Aley	9	24	48	73	97	328	820	1641	2461	3282	74	4.44
Saida	8	20	40	60	80	309	773	1547	2321	3095	73	4.24
Tyr	7	18	36	54	73	300	751	1503	2255	3006	124	2.42
Nabatiyé	6	16	33	50	67	286	715	1430	2145	2860	87	3.29
Kesrouane	7	17	35	52	70	255	639	1278	1917	2556	98	2.61
Békaa Ouest	9	23	47	71	95	201	504	1009	1514	2019	126	1.60
Beyrouth	18	46	93	139	**185**	181	453	907	1360	1814	**4**	**45.35**
Bent Jbail	6	17	34	51	68	163	409	818	1227	1637	80	2.05
Jbail	5	14	28	42	56	155	389	778	1167	1556	126	1.23
Minié-Danniyé	6	15	30	45	60	140	352	704	1057	1409	99	1.42
Koura	8	20	41	62	83	120	301	603	904	1206	49	2.46
Zgharta	7	18	36	55	73	107	269	539	809	1079	45	2.40
Batroun	5	14	29	43	58	104	261	523	784	1046	75	1.39
Tripoli	13	34	69	104	**138**	103	258	516	774	1032	**4**	**25.80**
Marjayoun	6	17	34	51	68	101	254	508	762	1017	74	1.37
Hermel	5	13	27	40	**54**	95	239	479	719	959	179	0.54
Rachaiya	7	19	39	59	78	95	238	477	716	954	184	**0.52**
Jezzine	6	15	31	47	63	62	155	311	467	623	64	0.97
Hasbaiya	8	20	40	60	80	53	133	266	399	532	78	**0.68**
Bcharré	5	13	27	41	55	35	88	176	265	353	41	0.86

Last column shows relative percentage of Total solar rooftop potential (at $U = 100\%$) with respect to the maximum hypothetical capacity (MWC in $TWh/year$) for each district. The table is sorted using TSP column in descending order.

highest GCR percentages (27.7% and 13.9%, respectively) as shown in Fig. 11.

Being extremely populated areas, Beirut and Tripoli districts have the highest average solar rooftop potential using a sliding window of surface $4Km^2$ as shown in Fig. 9(b). However, if shadowing effects were considered, one would expect lower average solar rooftop potential in these two high-density districts.

Baabda (1786 GWh/year), Aley (1641 GWh/year), Saida (1547 GWh/year), Tyr (1503 GWh/year), and Nabatiye (1430 GWh/year) districts show a large distribution of pink spots in Fig. 9(b). These districts are mid-populated areas (GCR values between 4% and 6%) with high PV_{out} values between 1700 and 1800 MWh/KWp. Using a 50% utilization factor, the total solar rooftop potential is fairly high in these districts and reach 3% to 4% of their maximum hypothetical capacity as shown in Table III.

Finally, Hermel, Hasbaya, Jezzine, Rachaiya, and Bcharre districts experience a blue tone in both Fig. 9(a) and (b). Average solar rooftop potential in those districts is poorly utilized, with less than $0.7\%\ GCR$ value. Total solar rooftop potential does not exceed 1% of each district's maximum hypothetical capacity.

We also provide in Table III detailed average and total solar rooftop potential for every district while varying the utilization factor from 10% to 100%. Assuming a 50% utilization factor, the total solar rooftop potential for all districts sums up to 28.1 TWh/year, whereas Lebanon total energy consumption

for the year 2019 (including Electricity of Lebanon, EDL, and private generators) was estimated by our EDL expert contact to be around 12.5 TWh/year. In the last column, we report $\%\frac{TSP}{HC}$ which constitutes the relative percentage of total solar rooftop potential (at $U = 100\%$) with respect to the maximum hypothetical capacity for each district. It is worth to note that $\%\frac{TSP}{HC}$ is directly proportional to GCR.

VII. CONCLUSION

We discussed in this article buildings' footprints segmentation for Lebanon from satellite imagery. We also computed solar rooftop potential using a panel fitting algorithm to produce the first complete solar potential map of Lebanon. Furthermore, we conducted rooftop- and district-level analysis to deduce patterns and provide policymakers and key stakeholders with tangible insights to design tailored regulations and future directions. We showed that 5% of the roof surface would be enough to accommodate the yearly electric needs of a single-family residence. As for residential apartments, the average solar rooftop potential using a 50% utilization factor is sufficient to provide up to 8 households with energy security. Baalbek district holds the highest total solar rooftop potential, while Beirut reports the highest average solar rooftop potential. We found that Lebanon's total solar rooftop potential is 28.1 TWh/year assuming a 50% utilization factor, which is more than double the national energy

consumption for 2019. Finally, we found that low-populated districts failed to deliver more than 1% of their maximum hypothetical capacity. Large solar farms are highly recommended solutions for Baalbek and Hermel districts to avail the high PV_{out} potentials.

Although our work leverages more accurate estimates of the rooftop potential than previous works for Lebanon, certain improvements can be further conducted concerning the buildings footprint extraction, panel placement algorithm, assessment of the actual roof utilization factor, and the PV_{out} map. For instance, in addition to the segmentation masks, we can estimate the building heights and the orientation of the points on the rooftops surface. This would eliminate the zero-shadowing and the orthogonal flat rooftop assumptions. Based on the heights, we can take shadowing effect between buildings into consideration. We can also reconstruct a 3-D surface of the rooftops given the orientation parameter, which would yield in a better estimate of the total available area of the rooftop, it's morphology and the presence of any obstacles. The panel placement algorithm can be improved by aligning the panels along the direction that maximizes the energy production as done in practice instead of aligning them along the main axis of the rooftop. Rooftop obstacles, best PV panel installation angle, and the spacing between the panels can be also taken into consideration to find the best distribution of the panels for each rooftop. An assessment study to find the actual rooftop utilization factor in Lebanon is essential to report practical figures. Such assessment would require first to generate ground truth labels using either remote sensing or field visits. Finally, the extraction of a higher resolution PV_{out} map is also key to attain more accurate results.

REFERENCES

[1] R. Alshehhi, P. R. Marpu, W. L. Woon, and M. D. Mura, "Simultaneous extraction of roads and buildings in remote sensing imagery with convolutional neural networks," *ISPRS J. Photogrammetry Remote Sens.*, vol. 130, pp. 139–149, 2017.

[2] Lebanese Center for Energy Conservation, "Availability, efficiency and use of home appliances in Lebanon: Results of survey of home appliances within retailers and households," Dec. 2020. [Online]. Available: https://lcec.org.lb/sites/default/files/2021-03/LCEC%20IEEHA%20REPORT%20E%20FOR%20WEB_1.pdf

[3] The United Nations Development Programme (UNDP)/CEDRO, "Photovoltaic power plants in Lebanon," Dec. 2013. [Online]. Available: http://www.databank.com.lb/docs/Photovoltaic%20plants%20in%20Lebanon-Cedro%202013.pdf

[4] Y. Chen, J. Li, H. Xiao, X. Jin, S. Yan, and J. Feng, "Dual path networks," in *Proc. Neural Inf. Process. Syst.*, 2017, pp. 4467–4475.

[5] D. de B. Soares *et al.*, "Predicting the solar potential of rooftops using image segmentation and structured data," in *Proc. Workshop Tackling Climate Change Mach. Learn.*, 2020.

[6] A. Dutta and A. Zisserman, "The VIA annotation software for images, audio and video," in *Proc. 27th ACM Int. Conf. Multimedia*, New York, NY, USA, 2019, pp. 2276–2279.

[7] H. Eslami, S. Najem, D. A. Ghanem, and A. Ahmad, "The potential of urban distributed solar energy in transition economies: The case of Beirut city," *J. Environ. Manage.*, vol. 285, 2021, Art. no. 112121.

[8] J. E. Fuentes, F. D. Moya, and O. D. Montoya, "Method for estimating solar energy potential based on photogrammetry from unmanned aerial vehicles," *Electronics*, vol. 9, no. 12, 2020, Art. no. 2144.

[9] The World Bank Group, "Global solar atlas 2.0: A free web-based application developed and operated by the company solargis S.R.O. on behalf of the world bank group, utilizing Solargis data, with funding provided by the Energy Sector Management Assistance Program (ESMAP)," 2019. [Online]. Available: https://globalsolaratlas.info

[10] K. He, X. Zhang, S. Ren, and J. Sun, "Deep residual learning for image recognition," in *Proc. IEEE Conf. Comput. Vis. Pattern Recognit.*, 2016, pp. 770–778.

[11] V. Iglovikov, S. Seferbekov, A. Buslaev, and A. Shvets, "Ternausnetv2: Fully convolutional network for instance segmentation," in *Proc. IEEE Conf. Comput. Vis. Pattern Recognit. Workshops*, 2018, pp. 233–237.

[12] S. Jadon, "A survey of loss functions for semantic segmentation," in *Proc. IEEE Conf. Comput. Intell. Bioinf. Comput. Biol.*, 2020, pp. 1–7.

[13] P. D. Kingma and J. Ba, "ADAM: A method for stochastic optimization," in *Proc. 3rd Int. Conf. Learn. Representations*, May 2015.

[14] W. Li, C. He, J. Fang, J. Zheng, H. Fu, and L. Yu, "Semantic segmentation-based building footprint extraction using very high-resolution satellite images and multi-source GIS data," *Remote Sens.*, vol. 11, no. 4, pp. 205–225, 2019.

[15] L. Mou, Y. Hua, and X. X. Zhu, "A relation-augmented fully convolutional network for semantic segmentation in aerial scenes," in *Proc. IEEE/CVF Conf. Comput. Vis. Pattern Recognit.*, 2019, pp. 12416–12425.

[16] E. Ng, C. Yuan, L. Chen, C. Ren, and J. C. H. Fung, "Improving the wind environment in high-density cities by understanding urban morphology and surface roughness: A study in Hong Kong," *Landscape Urban Plan.*, vol. 101, no. 1, pp. 59–74, May 2011.

[17] P. S. Prakash and H. B. Aithal, "A deep learning based approach for rooftop solar potential estimation of a city: A case study of indian metropolis," in *Proc. IEEE Int. Geosci. Remote Sens. Symp.*, 2021, pp. 8336–8339.

[18] J. Roerdink and A. Meijster, "The watershed transform: Definitions, algorithms and parallelization strategies," *Fundamenta Informatica*, vol. 41, no. 1/2, pp. 187–228, Jan. 2000.

[19] O. Ronneberger, P. Fischer, and T. Brox, "U-Net: Convolutional networks for biomedical image segmentation," in *Proc. Med. Image Comput. Comput.-Assist. Interv.*, 2015, pp. 234–241.

[20] Y. Shi, Q. Li, and X. X. Zhu, "Building extraction by gated graph convolutional neural network with deep structured feature embedding," in *Proc. IEEE Int. Geosci. Remote Sens. Symp.*, 2020, pp. 3509–3512.

[21] L. N. Smith and N. Topin, "Super-convergence: Very fast training of neural networks using large learning rates," in *Proc. SPIE 11006, Artif. Intell. Mach. Learn. Multi-Domain Operations Appl.*, May 2019, p. 1100612, doi: 10.1117/12.2520589.

[22] C. Szegedy, S. Ioffe, V. Vanhoucke, and A. A. Alemi, "Inception-v4, inception-resnet and the impact of residual connections on learning," in *Proc. 31st AAAI Conf. Artif. Intell.*, 2017, pp. 4278–4284.

[23] M. Tan and Q. Le, "EfficientNet: Rethinking model scaling for convolutional neural networks," in *Proc. 36th Int. Conf. Mach. Learn.*, 2019, pp. 6105–6114.

[24] M. Wei *et al.*, "Approaches to cost-effective near-net zero energy new homes with time-of-use value of energy and battery storage," *Adv. Appl. Energy*, vol. 2, 2021, Art. no. 100018.

[25] S. Xie, R. Girshick, P. Dollár, Z. Tu, and K. He, "Aggregated residual transformations for deep neural networks," in *Proc. IEEE Conf. Comput. Vis. Pattern Recognit.*, 2017, pp. 5987–5995.

[26] S. Yun, D. Han, S. Chun, S. J. Oh, Y. Yoo, and J. Choe, "Cutmix: Regularization strategy to train strong classifiers with localizable features," in *Proc. IEEE/CVF Int. Conf. Comput. Vis.*, 2019, pp. 6022–6031.

[27] T. Zhong *et al.*, "A city-scale estimation of rooftop solar photovoltaic potential based on deep learning," *Appl. Energy*, vol. 298, 2021, Art. no. 117132.
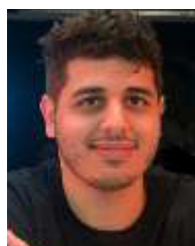
Hasan Nasrallah received the Diploma in computer and communications engineering from the Lebanese University, Beirut, Lebanon, in 2020.

He joined the Geospatial Earth Observation (GEO) Group as a machine learning assistant researcher and worked on several research topics related to deep learning, computer vision and remote sensing. In 2021, he joined Orbis Holding as a Machine Learning Engineer, where he is currently developing AI biometrics solutions for identity authentication, fraud prevention, and security. His areas of interest include artificial intelligence, computer vision and deep learning.

Abed Ellatif Samhat received the engineering diploma in electrical and electronics from the Lebanese University, Beirut, Lebanon, in 2000, and the master's and the Ph.D. degrees in computer science from Pierre et Marie Curie University, Paris, France, in 2001 and 2004, respectively.

From 2005 to 2008, he was a Research Engineer with France Telecom Group, Orange Labs–Paris, where he was involved in several national and European projects, including ambient networks and Gandalf. In 2009, he joined Lebanese University, where he is currently a Professor at the Faculty of Engineering. His areas of interest include heterogeneous wireless networks, IoT, and security.

Yilei Shi (Member, IEEE) received the Dipl.-Ing degree in mechanical engineering and the Dr.-Ing degree in signal processing from the Technische Universität München (TUM), Munich, Germany, in 2010 and 2019, respectively.

In April and May 2019, he was a Guest Scientist with the Department of Applied Mathematics and Theoretical Physics, University of Cambridge, Cambridge, U.K. He is a Senior Scientist with the Chair of Remote Sensing Technology, TUM. His research interests include fast solver and parallel computing for large-scale problems, high-performance computing and computational intelligence, advanced methods on synthetic-aperture radar (SAR) and InSAR processing, machine learning, and deep learning for a variety of data sources, such as SAR, optical images, and medical images, and partial differential equation (PDE)-related numerical modeling and computing.

Xiao Xiang Zhu (Fellow, IEEE) received the M.Sc., Dr.-Ing., and Habilitation degrees in signal processing from the Technical University of Munich (TUM), Munich, Germany, in 2008, 2011, and 2013, respectively.

She is a Professor of data science in Earth Observation (EO) (former: Signal Processing in EO) at TUM, and the Head of the Department "EO Data Science," Remote Sensing Technology Institute, German Aerospace Center (DLR). Since 2019, she has been a Co-Coordinator of the Munich Data Science Research School (www.mu-ds.de). Since 2019, she also heads the Helmholtz Artificial Intelligence–Research Field "Aeronautics, Space and Transport." Since May 2020, she has been the Director of the International Future AI Laboratory "AI4EO–Artificial Intelligence for Earth Observation: Reasoning, Uncertainties, Ethics and Beyond," Munich. Since October 2020, she has been a Co-Director of the Munich Data Science Institute (MDSI), TUM. She was a Guest Scientist or a Visiting Professor with the Italian National Research Council (CNR)-Institute for Electromagnetic Sensing of Environment (IREA), Naples, Italy; Fudan University, Shanghai, China; the University of Tokyo, Tokyo, Japan; and the University of California at Los Angeles, Los Angeles, CA, USA, in 2009, 2014, 2015, and 2016, respectively. She is a Visiting AI Professor at European Space Agency (ESA's) Phi-Laboratory. Her main research interests are remote sensing and earth observation, signal processing, machine learning, and data science, with their applications in tackling societal grand challenges, e.g., global urbanization, united nation (UN's) sustainable development goals (SDGs), and climate change.

Dr. Zhu is a member of the Young Academy (Junge Akademie/Junges Kolleg) at the Berlin-Brandenburg Academy of Sciences and Humanities and the German National Academy of Sciences Leopoldina and the Bavarian Academy of Sciences and Humanities. She serves in the Scientific Advisory Board in several research organizations, among others the German Research Center for Geosciences (GFZ) and the Potsdam Institute for Climate Impact Research (PIK). She is an Associate Editor of IEEE TRANSACTIONS ON GEOSCIENCE AND REMOTE SENSING and serves as the Area Editor responsible for special issues of the *IEEE Signal Processing Magazine*.

Ghaleb Faour received the Ph.D. degree in engineering science from the University of Marseille III - France, Marseille, France, in 1995.

He held a Researcher position from 1996 at the Lebanese National Center for Remote Sensing (CNRS) until he got promoted to become the Director of Research and the Director of the National Center for Remote Sensing in 2014. His main research interests focus on the development of applied remote sensing technology in the sector of environmental monitoring and natural resources management. He is a Lecturer in Remote Sensing and Geographic Information System at the Lebanese University and the Higher School of Surveyors and Topographers in Lebanon. He had supervised and co-advised more than 10 Ph.D. students and 20 Master Thesis. He conducted several specialized training courses and consultancies in GIS and Remote Sensing applied to urban planning, management of protected areas, agriculture, desertification, drought, climate change, and integrated water resources with the German International Cooperation (GIZ), UNDP, FAO and the Arab Institute of Forestry and Rangeland. He is the author of more than 50 articles published in peer-reviewed international journals as well as the co-author of *Atlas of Lebanon: Territory and Society* published in 2007 in French language and translated to Arabic in 2012, *Space Atlas of Lebanon* published in 2014 and *Atlas of Lebanon: New Challenges* published in 2016. He is the member of the National GIS Committee in 2002, the National Committee "Delimitation of the Maritime Exclusive Economic Zone" in 2009 and the Chairman of the National Committee "Unification of Geospatial Coding" in 2015, created by the Prime Minister Office. Also, he is the member of the Governing Board of the Regional Centre for Space Science and Technology Education for Western Asia located in Jordan. He is a national reference and representative of Lebanon in the United Nations Institutes UN SPIDER and UN Outer Space since 2010 in the sector of space research and activities.

Ali J. Ghandour received the Ph.D. degree in computer communication from the American University of Beirut (AUB), Beirut, Lebanon, in 2013.

He was with Toyota Motor North America, InfoTech Labs at Mountain View, USA, before joining CNRS in 2015, where he also acted as the coordinator of the Lebanese National Innovation Transfer Network. He is an Associate Researcher at the Lebanese National Center for Remote Sensing - National Council for Scientific Research (CNRS), where he established the Geospatial Earth Observation (GEO) Group.

He has more than 30 publications with unique research focus on AI-assisted mapping spanning various applications, including geospatial Earth observation, urban analytics, transportation, and features extraction from aerial imagery. GEO group develop tools integrating deep learning techniques to automate the process of urban features extraction and collect crowd-sourcing data from various sources. Evidence gained from GEO models and data analysis allows for a robust humanitarian response and provides policymakers and key stakeholders with insights to design tailored regulations and safety countermeasures for urban social good. In the past, he made research contributions to vehicular cognitive networks and IEEE P1609 standard Working Group.